

The Spacecraft Mass Balance as a Diagnostic Tool for Cabin Air Quality

Matthew J. Kayatin¹

NASA George C. Marshall Space Flight Center, Huntsville, AL, 35812, USA

The spacecraft-level mass balance is a powerful tool for diagnosing and decoupling factors influencing cabin air quality, especially with respect to trace contaminant propagation. Successful implementation of this approach relies upon accurate and temporally relevant air quality measurements, which are often challenging to attain for emerging trace contaminants. In addition to the proper interpretation of air quality data trends, a thorough understanding of subsystem-level mass transfer is required to characterize process performance. For many Environmental Control and Life Support System processes, subsystem mass transfer may be predicted based on physicochemical properties and classic unit operation design approaches. Gaps in understanding of process performance should be supplemented with thorough ground testing. A high confidence in the fidelity of one of these two aspects, air quality data or process performance, may help offset uncertainties in the other. At minimum, thresholding assumptions and numerical methods can be imposed to constrain unknown parameters within the physical envelope of the situation at hand. Finally, the complexity of cabin-wide integrated mass balances may be reduced by implementing a phenomenological approach towards subsystem discretization.

Nomenclature

<i>ECLS</i>	=	Environmental Control and Life Support
<i>C</i>	=	concentration of contaminant, mg/m ³
<i>CBA</i>	=	Charcoal Bed Assembly, ISS
<i>CCAA</i>	=	Common Cabin Air Assembly, ISS
<i>CHIPS</i>	=	Charcoal-HEPA Integrated Particle Scrubbers, ISS
<i>CHx</i>	=	Condensing Heat Exchanger
<i>COA</i>	=	Catalytic Oxidizer Assembly, ISS
<i>dev</i>	=	device
<i>g</i>	=	grams
\dot{g}	=	contaminant generation rate in mg/h
<i>HEPA</i>	=	high-efficiency particulate absorbing
<i>HVLA</i>	=	high velocity, low aspect-ratio
<i>I</i>	=	inter-module ventilation
<i>ISS</i>	=	International Space Station
<i>k_H</i>	=	Henry's law volatility constant
<i>LVHA</i>	=	low velocity, high aspect ratio
<i>m</i>	=	length, meter
η	=	single-pass removal efficiency
\dot{r}	=	effective contaminant removal rate, mg/h
<i>t</i>	=	time, hours (h)
<i>TCCS</i>	=	Trace Contaminant Control Subassembly, ISS
<i>THC</i>	=	temperature and humidity control
<i>V</i>	=	cabin free volume
\dot{v}	=	total subsystem, component, or device airflow rate, m ³ /h
<i>x</i>	=	mole fraction of contaminant in aqueous phase

¹ Lead Aerospace Engineer, ECLS Subsystems, Space Systems Dept., NASA MSFC/ES62

I. Introduction

THE impact of chemical or particulate leaks, spills, and releases on spacecraft cabin air quality may be predicted by contaminant propagation rates, in accordance with the overall spacecraft-level mass balances. Similarly, based on air-quality data trends, emerging contaminants may be analyzed and traced to better understand the magnitude of their release and therefore provide insight into their unknown origin using this approach. In either case, the accuracy and interpretation of these observations is predicated on a fundamental understanding of contaminant mass transfer at the Environmental Control and Life Support (ECLS) subsystem, component device level, or within spacecraft facility support equipment, combined with accurate air quality measurements. Often, the performance of the subsystem may be estimated using a traditional unit operations approach, supplemented when possible by property estimation tools or rigorous modeling and simulation. When correlations or relevant datasets are unavailable, ground testing must be implemented to derive process operating curves. In either case, the availability of relevant datasets may be quite dependent on the level of testing included within the subsystem or component's development lifecycle. This decision results in either a reactive or proactive posture in responding to an unexpected event such as a contaminant release or generation event. While the inclusion of rigorous component testing prior to flight is weighed against development cost and schedule margins, the risk of accepting a reactive vs proactive posture must also be considered. Time and cost savings realized up-front in the component development lifecycle may necessitate action on even tighter margins when problems arise in real-time and crew health is also of concern. Fortunately, the overall impact of these decisions may in certain cases be mitigated by the clever use of thresholding assumptions to simplify the analysis and reduce process performance unknowns. These special cases, combined with an approach to discretize subsystem performance in terms of the single-pass efficiency, simplifies the cabin-level mass balance such that rigorous performance calculations can be avoided. Additionally, numerical based approaches to diagnosing air-quality trends can, in certain scenarios, provide additional insight into the problem at hand.

II. The Cabin Mass Balance

For a fixed cabin volume (V) the change in concentration (C) of contaminant i with respect to time (t) is determined by the relative magnitude of the mass generation rate (\dot{g}) to the spacecraft's effective volumetric removal flow rate (\dot{r}). The product $\dot{r} \cdot C(t)$ defines the mass removal rate of contaminant. This relationship is described by Equation 1 and as written indicates that while \dot{r} is often constant for a contaminant, it is possible for \dot{g} to vary over time. Examples of practical release scenarios wherein the contaminant generation rate will be time variant include the evaporation of a shrinking liquid volume, venting of a pressurized gas through a restriction, and the overheating of electronics components¹. In case of a finite release of contaminant, $\dot{g} = 0$ and Eq. (1) is treated as an initial value problem with a well-known solution.²

$$V \cdot \frac{dC(t)}{dt} = \dot{g}(t) - \dot{r} \cdot C(t) \quad (1)$$

When investigating the emergence of new contaminant, a determination of $\dot{g}(t)$ is often of primary interest to help elucidate the origins of an unknown source. To simplify this approximation, it is preferred that data be scrutinized at steady state when the contaminant concentration has plateaued and subsystem telemetry has stabilized. At steady state, the cabin concentration is time invariant, and the final contaminant concentration is determined by the balance of \dot{g} and \dot{r} terms, as shown by Equation 2. Even if the cabin's stability is unknown, assuming a quasi-steady state around the time of air quality measurement is instructive as a first look at that time segment. This is possible due to the aforementioned stability in $\dot{r}(t)$, a result of operating against process control setpoints.

$$\dot{g} = \dot{r} \cdot C \quad (2)$$

By inspection of Eq. (2), an estimation of \dot{g} is dependent on the accuracy and availability of the air quality measurement for C . In other words, measurement tools capable of assessing unknown species are required to characterize emerging contaminants or unexpected releases. Also, it is notable that the spacecraft's volume does not impact the final steady-state condition, only the time dynamic. An understanding of the magnitude of the effective removal rate for each ECLS subsystem or incidental removal route is necessary, as defined by Equation 3. Herein, the effectiveness may be defined by the decimal single-pass removal efficiency (η) whose product with the bulk removal device airflow (\dot{v}) provides the effective contaminant "scrubbing" rate.

$$\dot{r} = \sum(\eta \cdot \dot{v}) \quad (3)$$

Defining the appropriate value of η for each subsystem and contaminant species is key to decoupling the chemical physics from Eq. (1). In this manner, subsystems are discretized from the overall calculation algorithm and the full utility of the spacecraft-level mass balance as a diagnostic tool may be realized.

A. Removal Efficiency

Anticipated removal efficiencies for several components are highlighted in Table 1. Examples include the following: 1) Active contamination control equipment such as Trace Contaminant Control Subassembly (TCCS) components, high-efficiency particulate absorbing (HEPA) filters, and the high velocity low aspect ratio (HVLA) Charcoal-HEPA Integrated Particle Scrubbers (CHIPS). Highlighted TCCS components include the low velocity high aspect ratio (LVHA) Charcoal Bed Assembly (CBA) as well as the high-temperature (temp.) Catalytic Oxidizer Assembly (COA). 2) Incidental contaminant removal routes include humidity condensate absorption occurring within temperature and humidity control (THC) equipment and leakage externally from the cabin via seals or airlocks. Highlighted is the Common Cabin Air Assembly (CCAA) which contains a co-current flow condensing heat exchanger (CHx) core.

The largest variability in component performance efficiency, according to Table 1, is expected for condensate absorption and HVLA adsorption-based processes. Anticipated process performance for TCCS components and detailed methodology for predicting process operating curves for condensate absorption was addressed by Perry and Kayatin (2016).³ Experimental performance characteristics for HVLA adsorption architectures as a function of Polanyi adsorption potential energy can be found in Kayatin and Perry (2017).⁴

B. Sensitivity and Uncertainty

The range of η for various processes, as shown by Table 1, can have a significant impact on the predicted value of \dot{g} under a sustained contaminant release scenario. Figure 1 highlights the dependence of \dot{g} on \dot{r} over a range of C from 0.1 to 1.0 mg/m³. While the estimated magnitude of \dot{g} varies with \dot{r} for a fixed contaminant concentration level (i.e. $C = \text{constant}$), it follows that uncertainty within the value of \dot{r} is dependent on the accuracy of η (see Eq. (3)). The sensitivity of the predicted \dot{g} , however, is ultimately dependent on the magnitude of the various component flowrates. In other words, when devices with larger \dot{v} contribute to clean-up, the error in \dot{g} may be large. This effect is magnified at a higher sustained cabin C .

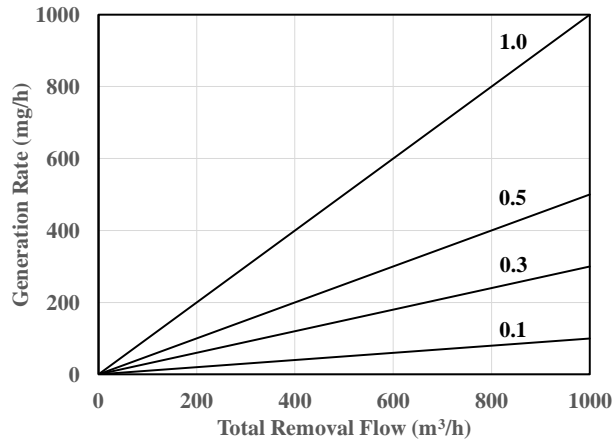


Figure 1. Dependence of predicted contaminant generation rate on total removal flow at a fixed cabin concentration (0.1 – 1.0 mg/m³).

Table 1. Summary of common removal device operations, configurations, and expected efficiencies.

Operation	Configuration	Example	η (%)
Adsorption	LVHA	TCCS CBA	0 or 100*
Adsorption	HVLA	CHIPS	0 – 100
Oxidation	High-temp.	TCCS COA	> 90*
Absorption	Co-current	CCAA CHx	0 – 100
Filtration	Pleated	HEPA	> 99.9
Leakage	External	Seals	100

*idealized. †For COA design driving compounds.²

III. Special Cases

Several scenarios are commonly encountered wherein simplifying assumptions may be made to reduce the uncertainty in component efficiencies highlighted by Table 1. These include the two extremes of a release being characterized by a relatively low and high adsorption potential energy, which allows for assumption of zero or complete capture efficiency on activated carbon, and a release of contaminant with limited water solubility such that condensate absorption may be ignored. These special cases are discussed further below.

A. Simplifying Thresholds for Adsorption

The Polanyi adsorption potential has been introduced in detail elsewhere.^{3,4} Briefly, the adsorption potential energy may be interpreted as the thermodynamic work

required to move a contaminant from the vapor to adsorbed phase. At constant temperature, the potential function is the product of inverse and logarithmic mathematical relations. Specifically, the adsorption potential is sensitive to inverse molar volume and its magnitude is typically dominated by small molecules due to the divergent behavior of this inverse function compared to its logarithmic component. This behavior mathematically characterizes the inability of activated carbons to capture permanent or non-condensable gases at high capacity and gives context to the assumption of selecting zero adsorption efficiency for a chemical compound. Conversely, the adsorption of large molecules, often also aided by low or diminishing vapor pressures, can be characterized to occur with low adsorption potential energy such that the performance of an adsorption-based process may be assumed to be 100% efficient. In this case, the total mass of the release relative to the anticipated adsorption capacity for the removal device must also be taken into consideration. When the chemical release is expected to approach the saturation capacity of the adsorption bed, process inefficiencies associated with breakthrough should also be considered.

B. Simplifying Threshold for Absorption

The delineation between water-soluble and insoluble compounds must be taken in context with the operating line of the CCAA CHx as well as the typical detection limits for contaminants in humidity condensate grab samples.³ The historical reporting limit for common polar organics (alcohols & acetone) in condensate grab samples was recently on the order of 0.4 mg/L according to internal NASA water quality reports. Assuming a contaminant release into cabin atmosphere of 1 mg/m³, the condensate temperature adjusted Henry's law volatility constant (k_H) must decrease to approximately 3 atm/x, where x is defined as the mole fraction of contaminant in the aqueous phase, to meet these reporting limits. Broadly speaking, a general recommendation may be to classify compounds with temperature adjusted $k_H > 10$ atm/x as insoluble when characterizing the mass transfer from vapor to liquid by condensate absorption. Note that the analogous Henry's law solubility constant (dimensions of aqueous concentration/partial pressure) is not amenable to temperature adjustment and care must be taken to not confuse the two values. Ultimately, if the total air flow through the condensing unit operation is large enough, even compounds with diminishing η may have a relevant total mass absorbed and this diagnostic should be checked on a case-by-case basis.

C. Recommended Future Work

Due to the limited availability of published datasets describing adsorption breakthrough and mass transfer coefficients at high velocities, the performance of CHIPS filters for trace contaminants is at present best determined by ground testing rather than by predictive modeling. Recently (2020), an internal literature review to help predict the performance of CHIPS for trace benzene adsorption found a deficiency in published intra-particle mass transfer coefficients at the process operating flowrate. Generation of adsorption breakthrough datasets for various trace contaminants at high velocity would help supplement this gap. Furthermore, the favorable kinetics⁴ towards capturing contaminants with low adsorption potential energies introduces additional complexities from competitive adsorption phenomena that may depend on the carbon exposure history and whose prediction is still an ongoing area of research.⁵

Trends in commercial vehicle THC architectures appear to favor open-loop, permeation based dryers over condensation based dehumidification.⁶ To this end, the selective permeability of water vapor through various Nafion element geometries is utilized by leveraging partial pressure gradients across the vacuum of space. Rigorous ground testing with simulated trace contaminant loads relevant to manned spacecraft, and careful trace contaminant measurements, will help determine the removal efficiencies in these devices.⁷ An understanding of contaminant mass transfer in these architectures will be required to effectively implement spacecraft-level mass balances as a diagnostic tool on commercial spacecraft as well.

IV. Diagnostic Tools

With the fundamental mass balance expressions defined, and component performance and thresholding assumptions addressed, the implementation of two diagnostic tools may be demonstrated by mathematical simulation of cabin behavior under certain scenarios. The desired outcome of the exercise is the estimation of the magnitude of an unknown contaminant generation rate, source location, and total mass of contaminant released.

A. Segmented Mass Balances

The dispersion of contaminant i between two adjacent spacecraft modules, having fixed free volumes, V_A and V_B , with active contamination control equipment, may be described by Equations 4 and 5. Here, the modules are exchanging mass via inter-module ventilation (\dot{I}) wherein \dot{I}_A and \dot{I}_B represent cabin airflow exiting V_A and V_B , respectively. Additionally, the total effective contaminant removal flow for each module is specified by $\dot{r}_{i,A}$ and $\dot{r}_{i,B}$

with local contamination generation rates specified by $\dot{g}_{i,A}$ and $\dot{g}_{i,B}$. These expressions are valid when the individual segments are assumed or verified to be instantaneously well-mixed.

$$\frac{dc_{i,A}}{dt} = \frac{1}{V_A} \cdot [J_B \cdot C_{i,B} - J_A \cdot C_{i,A} - \dot{r}_{i,A} \cdot C_{i,A} + \dot{g}_{i,A}] \quad (4)$$

$$\frac{dc_{i,B}}{dt} = \frac{1}{V_B} \cdot [J_A \cdot C_{i,A} - J_B \cdot C_{i,B} - \dot{r}_{i,B} \cdot C_{i,B} + \dot{g}_{i,B}] \quad (5)$$

Simultaneous solution of Eq. (4) and Eq. (5) results in the time-dependent concentration profiles of i in segment A ($C_{i,A}$) and B ($C_{i,B}$), respectively. Analytical solutions to these simultaneous differential mass balances was provided by Perry (2005).⁸ To simplify this process, these expressions are solved numerically herein. The resulting dispersion profiles are valuable in predicting the propagation of a contaminant release between spacecraft modules. By setting the initial condition in the segment containing the spill to be that of the well-mixed contaminant concentration, time dynamics of dispersion to the adjacent spacecraft segment may be tracked. Less apparent, however, is the utility of these expressions in helping determine the magnitude of \dot{g}_i for an unknown contaminant release or spill; this will further be demonstrated by the examples herein.

Consider the following example wherein an 800 m³, two-module spacecraft is experiencing an anomalous particle generation event with unknown generation rate and undetermined source location (i.e. segment A or B). Assume the spacecraft's particle detector was able to document the emergence of the contaminant as shown by Figure 2. The cabin atmosphere is assumed to be instantaneously mixed within each segment but not necessarily well-mixed across the entire spacecraft. The average steady state concentration was 0.23 mg/m³. Segment A has a free volume of 200 m³ and is equipped with a HEPA filtration element capable of removing detectable particulate with $\eta > 99\%$ such that $\dot{r}_{i,A}$ is confidently known based on the nominal filtration air flow (let $\dot{v}_A = 25$ m³/h). Unfortunately, the performance of Segment B's particulate removal efficiency is unknown, akin to the uncertainties discussed with certain processes in Table 1. Segment B has a free volume of 600 m³ and contains several ECLS subsystems with a total influent flow of 400 m³/h (i.e. let $\dot{v}_B = 400$ m³/h). The magnitude of \dot{r}_i for the full cabin ultimately depends on the slack in η and therefore the value of $\dot{r}_{i,B}$. In this scenario, the overall contaminant generation rate cannot be accurately estimated due to the uncertainty in $\dot{r}_{i,B}$. If the value of η ranges from 0 to 100% then $\dot{r}_{i,B}$ ranges from 0 to 400 m³/h and the overall range in \dot{r}_i for the total cabin from 25 to 425 m³/h. Estimating the value of \dot{g} in accordance with Eq. (2) therefore results in a range from 25·C to 425·C which is equivalent to approximately 6 to 100 mg/h using the steady-state load. This range of uncertainty (74 mg/h) in estimated magnitude may cause confusion and mask the origin of the contaminant source, leading to additional diagnostic problems. Furthermore, no apparent insight into the location of the source is available from this analysis alone.

To reduce uncertainty in the performance of the Segment B removal flow, subsystems may be challenged via a rigorous ground test intended to mimic the conditions exhibited on the spacecraft. Similarly, modeling and simulation-based approaches may be employed to constrain the range on unknowns using physical or chemical arguments. Both

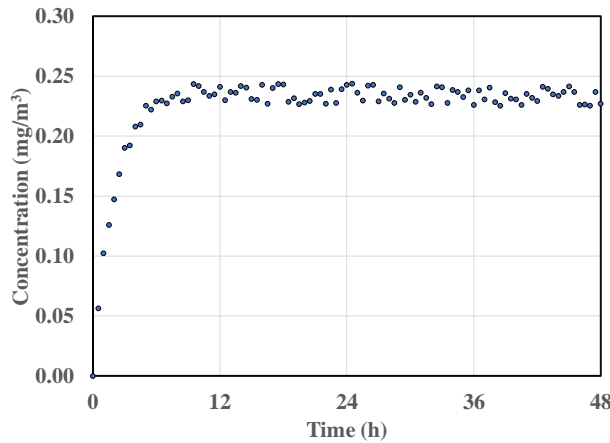


Figure 2. Detected contaminant concentration profile in a well mixed 800 m³ cabin.

approaches necessitate the expenditure of time and resources and this may or may not be acceptable depending on whether crew health is at question due to the emerging contamination event. Alternatively, probing the two spacecraft segments separately, either analytically or with the help of active investigation, may give more insight into the possible location and magnitude of a point source. This may be achieved by routing sample plumbing, capturing isolated grab samples, or physically moving the detector throughout the cabin volume with the hope of measuring local concentration gradients. It is quite possible, however, that the spatial differences in contaminant concentration between two exchanging segments is minimal or within the error of the detector used. The expected magnitude of the contaminant gradient will depend on several parameters such as the segment's relative balance between contaminant generation and removal rates and

the rate of inter-module ventilation. Therefore, the utility of this approach may be further enhanced by reducing or eliminating inter-module ventilation and/or enabling/disabling additional scrubbing flow. As described by Eq. (4) and Eq. (5), setting \dot{I}_A and \dot{I}_B to zero reduces these equations to a form like that of Eq. (1). Mathematically, this can eliminate mass transfer away from the segment containing the contaminant source by bulk flow and allow enough time for clean-up in the now isolated adjacent module. Analysis of the time dynamics of the clean-up, for example, may remove or reduce any uncertainty associated with unknown removal flow performance. The exact result will depend on the model input parameters outlined above and will be further demonstrated below.

To continue the example, assume the inter-module ventilation is well matched in each direction at approximately $170 \text{ m}^3/\text{h}$ (i.e. $\dot{I}_A = \dot{I}_B$). Furthermore, allow a point source to exist such that $\dot{g} = 100 \text{ mg/h}$ (unknown to the analyst or reader) for the purpose of simulating cabin behavior to analyze. To illustrate some of the anticipated subtleties within the distributions, it is now briefly assumed the contaminant is effectively removed everywhere throughout the cabin ($\eta = 100\%$). The effective removal flow is therefore much higher in Segment B with $\dot{r}_{i,B} = 400 \text{ m}^3/\text{h}$ as compared to that of Segment A where $\dot{r}_{i,A} = 25 \text{ m}^3/\text{h}$. The predicted segment concentration profiles, depending on the location of the source, are shown by Figure 3 and Figure 4.

In Figure 3, the point-source is located within the larger Segment B, which also contains a relatively large contaminant scrubbing capacity such that bulk mass transfer from B to A is limited. The resulting concentration profiles are therefore very similar in shape and steady-state magnitude. In this case, relocating the particle detector may not yield any meaningful or new data regarding the source. The final steady-state concentrations are 0.21 mg/m^3 and 0.24 mg/m^3 in Segment A and B, respectively.

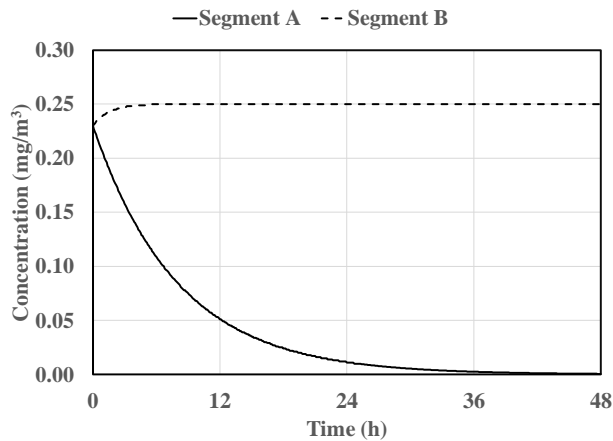


Figure 5. Predicted isolated segment contaminant profiles when Segment B contains the source.

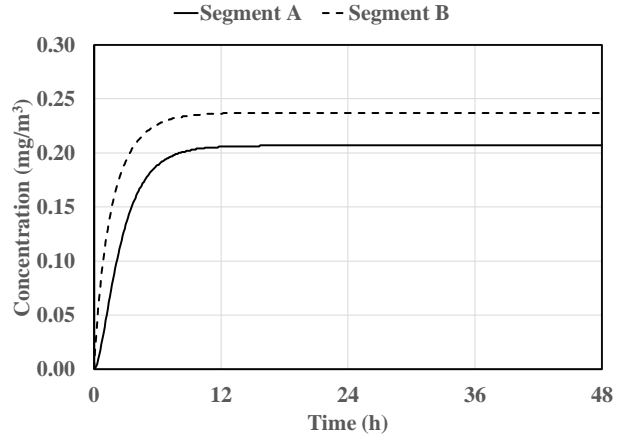


Figure 3. Predicted contaminant dispersion profiles when Segment B contains the source.

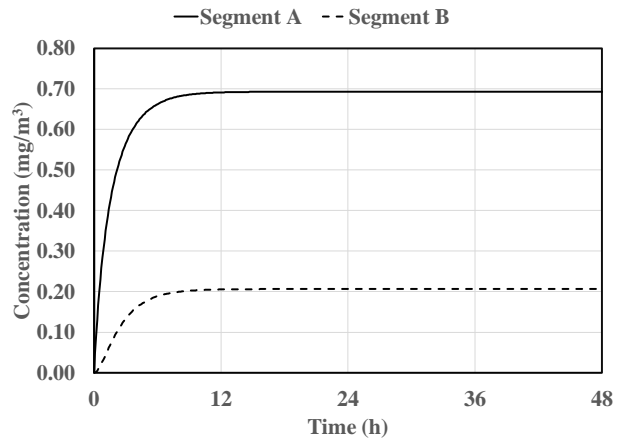


Figure 4. Predicted contaminant dispersion profiles when Segment A contains the source.

In Figure 4, the example is reversed by instead moving the point-source to be within Segment A, which contains smaller contaminant removal flow respective to B. In this case, bulk mass transfer from segment A to B is significant. The disparity in contaminant load between the segments is also apparent with the final steady-state contaminant concentrations being 0.69 mg/m^3 and 0.21 mg/m^3 in Segment A and B, respectively. This concentration difference provides insight into the location of the contaminant source.

Furthermore, to illustrate the utility of isolating segments, allow $\dot{I}_A = \dot{I}_B = 0$. Consider again the case with a source located in Segment B. As shown by Figure 5, the spacecraft transitions away from a well-mixed cabin, as was highlighted in Figure 2 ($t > 6 \text{ h}$), with an initial condition of approximately 0.23 mg/m^3 . Clearly, by the observed trends displayed by Figure 5, the source

was in fact located in Segment B since the contaminant concentration in Segment A exhibits the expected exponential decay predicted by the analytical solution to the Eq. (1) initial value problem. The result of this experiment is confirmation on the location of the contaminant source. While the decay rate in Segment A may also be used to validate the anticipated performance of the contaminant removal systems therein, it has not provided any additional insight needed to close any uncertainty regarding the performance of the scrubbing in Segment B. Recall, that initially the example for the mixed cabin included unknown scrubber performance in this segment. If instead the performance of the scrubbing in Segment B is assumed known, then the estimated generation rate based on the final steady-state cabin concentration of 0.25 mg/m^3 was therefore $C \cdot (\dot{r}_{i,B})$ or 100 mg/h , which matches the upper end of the anticipated range of uncertainty in \dot{g} . If instead the performance of $\dot{r}_{i,B}$ is unknown, nothing further may be learned from this scenario besides the source location and an alternative approach to estimate \dot{g} is required.

Repeating the module isolation experiment for the case when the source is instead isolated to Segment A, the trends for each module are reversed and the outcome is more instructive towards $\dot{r}_{i,B}$. In this case exponential decay is rapidly observed in Segment B, and regression of the observed concentration trend may be analyzed to extract any unknown η . Furthermore, with the source isolated to Segment A, having a relatively low contaminant scrubbing rate ($25 \text{ m}^3/\text{h}$), the observed concentration growth dynamic may now be analyzed to estimate the source generation rate. If this experiment runs long enough to reach steady-state, \dot{g} may be simply estimated as $C \cdot \dot{r}_{i,A}$ by utilizing the cabin's plateau concentration. As shown by Figure 6, the change in concentration dynamics are quite apparent with a steady-state concentration of 4 mg/m^3 , resulting again in a 100 mg/h source rate.

Alternatively, \dot{g} may be estimated by Eq. (2) for the combined cabin now that any uncertainty in $\dot{r}_{i,B}$ has been removed (if necessary) from Eq. (3) by again utilizing the bulk dataset shown by Figure 2. The estimated generation rate based on the steady-state cabin concentration of 0.23 mg/m^3 was therefore $C \cdot (425 \text{ m}^3/\text{h})$ or 97.8 mg/h , which matches the upper end of the anticipated range of uncertainty in \dot{g} . This result is expected since the value of η was assumed *a priori* for the purpose of this illustration. Nevertheless, the example is instructive as to how a real dataset may be analyzed and the results interpreted for several scenarios.

The practice of isolating segments must also take into consideration risk to crew health and decisions should be made to limit crew exposure in isolated segments with relatively low scrubbing potential. This was demonstrated by the concentration dynamic for Segment A in Figure 6. The predicted steady-state concentration in that segment should be compared to applicable crew exposure guidelines. Additionally, if the detector may not be relocated then options for making changes or adjustments to removal flow with known performance parameters can also help reduce uncertainty by starting or stopping subsystem operations.

B. Mass Accounting

The total magnitude of a spill or release may be extracted from the measured contaminant concentration profile to gain insight into potential source origin. Realistic scenarios capable of generating a hypothetical release mass having similar order of magnitude may then be explored. This process is straightforward for steady-state concentrations with well described cabin effective removal rates and only slightly more tedious when data trends are not monotonic in nature. Formally, the mass scrubbed over time interval $[a, b]$ can be described by the definite integral of the product $\dot{r} \cdot C(t)$, as shown by Equation 6 and generally written for each removal device (*dev*). When constant, \dot{r}_{dev} may be removed from the integrand leaving only the integral $C(t) dt$ to be evaluated. This integral may be approximated numerically from the contaminant concentration profile in accordance with the trapezoidal rule as shown by Equation 7.

$$r_{dev} = \int_a^b \dot{r}_{dev} \cdot C(t) dt \quad (6)$$

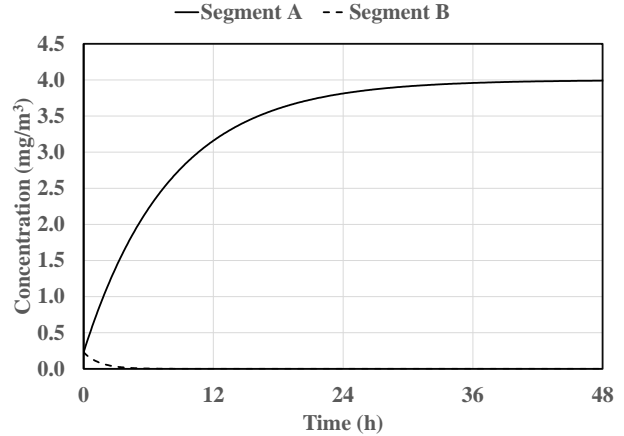


Figure 6. Predicted isolated segment contaminant profiles when Segment A contains the source.

$$\int_a^b C(t) dt \approx (b - a) \cdot \left(\frac{C(a)+C(b)}{2} \right) \quad (7)$$

Consider as an example the exercise in calculating the total contaminant mass released over 48 h from the concentration profile shown within Figure 2. Assume a well-mixed cabin (800 m^3) which contains a scrubber operating with an effective removal flow of $425 \text{ m}^3/\text{h}$. As a first approximation, an upper limit to the total mass captured in the device [$\dot{r} \cdot C \cdot \Delta t$] may be estimated by utilizing the steady state cabin concentration (0.23 mg/m^3) to find a mass of 4692 mg . Note that this overestimates the release since the growing concentration dynamic over the first 9 h is not captured. Application of Eq. (6) to the dataset finds a more accurate release estimate of 4597 mg . In either case, note that these estimates are significantly greater than the 184 mg of contaminant dispersed within the steady state cabin atmosphere ($V \cdot C$), showing how important accounting for device captured mass is in describing a release. This is even more pronounced when multiple devices or routes capable of capturing the contaminant are present. Often the mass of contaminant dispersed in the atmosphere is thought to be most indicative of the spill quantity, but this is an oversight. As shown in this example, the total magnitude of the release can be incorrectly interpreted by this misunderstanding. Nonetheless, with this information, the pure component density, and physical state, certain credible contaminant release scenarios may be identified. Furthermore, once the magnitude of the total mass captured has been estimated, dividing by the time duration generates a rough estimate of the contaminant generation rate (assumed to be constant) as 96 mg/h . This serves as a second method to check the predicted contaminant generation rate.

V. Conclusion

The spacecraft-level mass balance is a powerful tool for diagnosing factors influencing cabin air quality such as the propagation of contaminant releases or spills. While accurate air quality measurements are required for analysis, a detailed understanding of the subsystem-level mass transfer or performance is essential. For many ECLS processes, the effective removal rates may be predicted based on physicochemical properties and classical unit operation approaches. Otherwise, ground testing of components is required to supplement data gaps in process performance. With this in mind, some recommendations were made for future studies on two specific ECLS components. Often, simplifying assumptions may be implemented to threshold anticipated component performance, as was discussed for adsorption and absorption-based processes. An understanding of the basic subsystem-level mass transfer allows for implementation of a more complex mass-balance diagnostic approaches. To this end, simulated cabin behavior for contaminant generation into a segmented cabin were discussed and a numerical approach to estimate the total contaminant mass of a release was demonstrated. With command of these techniques, the contaminant generation rate from an unknown release or spill can be estimated to better understand the magnitude and source of the event within spacecraft.

Acknowledgments

Thank you to Jay L. Perry for invaluable guidance and insight. Thank you to Stephanie N. Roohi and Kevin E. Lange for investigating predictive mass transfer kinetics in high velocity filters. Thank you to Oscar Monje and J. Riley Finn for the generation of relevant adsorption datasets. Thank you to Elizabeth M. Bowman for brainstorming and sharing chemical intuition. Finally, thank you to Stephen Tyson for collaboration and insight during the implementation of these numerical techniques for diagnosing the International Space Station (ISS) in 2020.

References

- ¹Kulis, M.J., Meyer, M.E., Mudgett, P.D., Berger, G.M., and Pilgrim, J.S., "Heating of Printed Circuit Board, Wire Insulation and Electronic Components for Fire Signature Sensor Evaluation," *44th International Conference on Environmental Systems*, ICES-2014-87, Tucson, Arizona, 2014.
- ²Perry, J. L., "Elements of Spacecraft Cabin Air Quality Control," *NASA/TP-1998-207978*, May 1998, pp. 139.
- ³Perry, J. L. and Kayatin, M. J., "The Fate of Trace Contaminants in a Crewed Spacecraft Cabin Environment," *46th International Conference on Environmental Systems*, ICES-2016-91, Vienna, Austria, 2016.
- ⁴Kayatin, M. J. and Perry, J. L., "Evaluation of a Candidate Trace Contaminant Control Subsystem Architecture: The High Velocity, Low Aspect Ratio (HVLA) Adsorption Process," *47th International Conference on Environmental Systems*, ICES-2017-257, Charleston, South Carolina, 2017.
- ⁵Roohi, S. N., Kayatin, M. J., Perry, J. L., and Lange, K. E., "Dynamic Modeling of Gaseous Multicomponent Trace Contaminant Adsorption," *49th International Conference on Environmental Systems*, ICES-2019-238, Boston, Massachusetts, 2019.

⁶Iacomini, C. S., Harrell, J. and Lopez, J., "Nafion Bundle Technology for Space Flight Humidity Control," 45th *International Conference on Environmental Systems*, ICES-2015-153, Bellevue, Washington, 2015.

⁷Perry, J. L. et al., "Evaluation of an Atmosphere Revitalization Subsystem for Deep Space Exploration Missions," 45th *International Conference on Environmental Systems*, ICES-2015-107, Bellevue, Washington, 2015.

⁸Perry, J. L., "Formaldehyde Concentration Dynamics of the International Space Station Cabin Atmosphere," *SAE Technical Paper*, No. 2005-01-3091, 2005.